

Observational Study of the Surface Layer at an Ocean–Land Transition Region

Luiz Eduardo Medeiros¹, Roberto de Oliveira Magnago², Gilberto Fisch¹, Edson Roberto Marciotto¹

ABSTRACT: High-frequency measurements of wind, and temperature were made during the dry season of 2008 to study the development of an internal boundary layer at the main Brazilian space launching centre, Centro de Lançamento de Alcântara at Alcântara, Maranhão, Brazil. Turbulence measurements taken at the coast, in two different points 227 m apart show different daily cycles of turbulent kinetic energy friction velocity (u_*), and buoyancy flux $\overline{w'T_v'}$. Surface roughness change, surface heating change, and a gap in the natural vegetation seem to be the causes for the variation in these turbulent parameters. The mean wind cycle also shows distinct patterns. It seems that, first, internal boundary layers develop when the oceanic surface layer reaches the continent, and a second when the first internal boundary layer's flow encounters the gap. A direct implication is that turbulence is not horizontally homogeneous and measurements taken at single places are not spatially representative. Knowing how turbulence varies spatially is necessary information to understand the diffusion of pollutants exhausted by rockets near the coast.

KEYWORDS: Coast, Internal boundary layer, Sonic anemometer, Surface layer.

INTRODUCTION

The space vehicle launching centers are usually located at coastal areas due to safety reasons. Examples are the Kennedy Space Centre at Florida, Centre Spatial Guyanais at French Guiana, and Centro de Lançamento de Alcântara (CLA) at Brazil, all of which are located on the coast. CLA, for instance, has its launching pad around 650 m from the seashore. At the coastal regions there are always surface cover changes and in some case changes in topography too. Changes in surface cover create discontinuities in surface roughness and heating, which in conjunction with the topography affect the distribution of winds, temperature, and humidity. It is well known that boundary layers being advected over surface with discontinuities develop internal boundary layers (IBL) (Stull, 1988; Arya, 2001).

A boundary layer is the layer of fluid near a boundary that is affected by friction against that boundary surface, and possibly by transport of heat and other variables across that surface. An IBL is a layer within the atmosphere bounded below by the surface, and above by a more or less sharp discontinuity in some atmospheric property. A surface layer is the same as a surface boundary layer, which is a layer of air of order tens of meters thick adjacent to the ground where mechanical (shear) generation of turbulence exceeds buoyant generation or consumption.

In the case of roughness discontinuities, the mechanically generated IBL might reach equilibrium within or less than a kilometer downwind from discontinuity and its effects are likely to be felt only at the surface layer. In case of surface heating discontinuity, the internal boundary layer might reach equilibrium only at much larger distances (Garratt, 1990;

¹Instituto de Aeronáutica e Espaço – São José dos Campos/SP – Brazil ²Universidade do Estado do Rio de Janeiro – Resende/RJ – Brazil

Author for correspondence: Roberto O. Magnago | Departamento de Matemática, Física e Computação/Faculdade de Tecnologia/Universidade do Estado do Rio de Janeiro | Rodovia Presidente Dutra km 298 – Pólo Industrial | CEP 27.537-000 Resende/RJ – Brazil | Email: ducamobi@gmail.com

Received: 21/03/13 | Accepted: 26/07/13

Mahrt and Vickers, 2005) and it may affect much deeper layers. Sea and land breezes are examples of thermal IBLs. On this regard, Case *et al.* (2005) analyzed the sea breeze climatology at Kennedy Space Centre using a network of 44 mesonet towers and five wind profiles, while Merceret (2006) studied the rapid temporal variation of the winds using wind profilers. For the case of CLA, Gisler *et al.* (2011) studied the climatology of the surface winds through 5 years of data from a 70 m-high anemometric tower, in order to characterize the wind flow regime in the region. Recently, Moreira *et al.* (2011) described the usage of a software to study the dispersion of pollutants (or toxic gases) released at CLA.

The CLA is located in the northeast (NE) of Brazil, right at the shoreline. The wind regime at its location is influenced by the trade winds and perhaps by a sea/land breeze circulation (Gisler *et al.*, 2011). Besides these influences, there is also influence from a topographic barrier, an escarpment. The barrier is located just where the beach ends, and according to a wind tunnel study/simulation carried by Marinho *et al.* (2009), the flow is supposed to accelerate around the edge of the escarpment and to develop a recirculation a few hundred meters downwind from it. The limitation of this study is that the escarpment was approximated by a step-like barrier with 90 degrees inclination, which is not realistic. The understanding of how the marine boundary layer is affected, and how the surface layer is modified downwind from the escarpment, is extremely important for the evaluation of the stress caused by turbulence and wind on the structure and trajectory of rockets, well as for the dispersion of pollutants exhausted by them.

For the region of CLA, mechanical and thermal IBLs should be developed when the marine boundary layer reaches the coast. Nonetheless, in this work we focus only on the mechanical effects exerted on the near-surface turbulence. The possible deeper effects of the surface heating discontinuity on the local planetary boundary layer are left for a future work.

DATA

Most of the data used in this work are from the Murici II meteorological campaign (Marciotto *et al.*, 2012) conducted at CLA, during September 17–25 of 2008. The measurements were taken right at the coast. The transition zone water-land

is composed by an eroded slope about 40 m high, very heterogeneous, which at some points resembles cliffs. The slope is partially vegetated and delimitates the border of a plateau. In Fig. 1, it is shown that the slope with the surface cover change from water to land with small dense bushes typically 3 m tall. In Fig. 2 the local topography with the plateau and the surrounding slope is shown. The topographic surface (Fig. 2) was built using data from the Shuttle Radar Topography Mission provided by NASA Land Processes Distributed Active Archive Center (<http://gdex.cr.usgs.gov/gdex/>). The spatial resolution is 3 arc-seconds or approximately 92 m for Alcântara region.

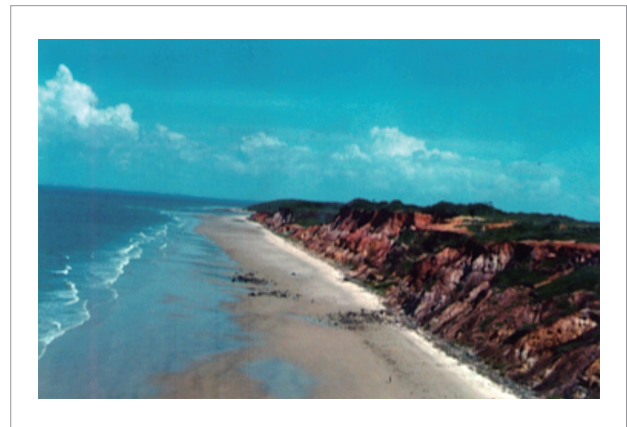


Figure 1. The topographic barrier between the ocean and the plateau, the escarpment.

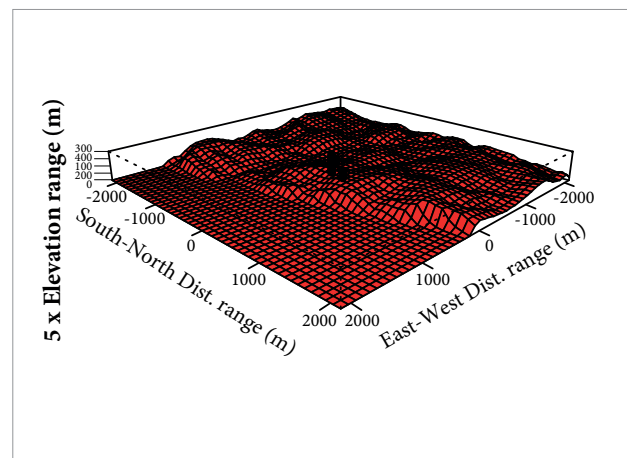


Figure 2. A perspective of the topographic of the region with respect to the prevailing wind direction. The taller vertical segment indicates the position of the tower plus Sonic B, and the shorter segment the mast with Sonic A. The flat part of the surface corresponds to the sea.

Measurements were taken at approximately 675, 700, and 750 m inland at the plateau, as shown in the terrain cross sections (Fig. 3) along the direction of the prevailing wind during the time of the experiment – NE (Fig. 4). The Shuttle Radar Topography Mission data produces very similar cross

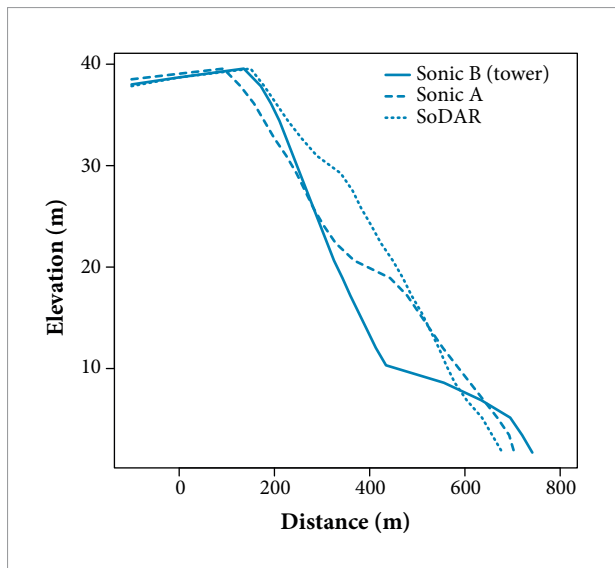


Figure 3. Cross section of the terrain's elevation through Sonic A, Sonic B, and SoDAR, along the prevailing wind direction (NE). Zero in x-axis refers to the exact sensors' position, right x-axis refers to upwind distance, and left x-axis to downwind distance. The elevation data were obtained from a local topographic map.

sections like the ones presented in Fig. 3; however, we preferred to use a local topographic map because there was more data in the region of the slope. The windroses presented in Fig. 4 show the prevailing wind direction in the region. For their determination we used 30 minutes average of zonal (u) and meridional (v) wind components during the period of the experiment. There are 16 directional sectors for each windrose, and every sector corresponds to a range of 22.5 degrees.

At 750 m inland there was a 70 m tall tower (taller vertical segment in Fig. 2) with a wind profile composed by six propeller anemometers at the levels 6, 10, 16, 28, 43, and 70 m. A 3D sonic anemometer (Sonic B), from Campbell Scientific, Inc. (model CSAT3), was mounted on the tower at 9.5 m above ground level (AGL). Gisler *et al.* (2011) describes some climatological features of this tower. At 700 m inland, there was a second sonic anemometer (Sonic A – shorter segment in Fig. 2) installed at 9.5 m (AGL) on a mast. This site was located in a clearing with sparse small grass. The clearing, with Sonic A behind, is shown in Fig. 5 upper panel. The prevailing wind direction is from the bushes on the right side of the picture. The upwind natural vegetated fetch of Sonic B is presented in the lower panel of Fig. 5. The sonic boom points towards the direction from where the wind comes from.

The broader view of the details of the landscape of the region, where the tower and Sonic A were located, is presented in an aerial photo of the region (Fig. 6). Inside the clearing, where Sonic A was located with respect to the direction of the

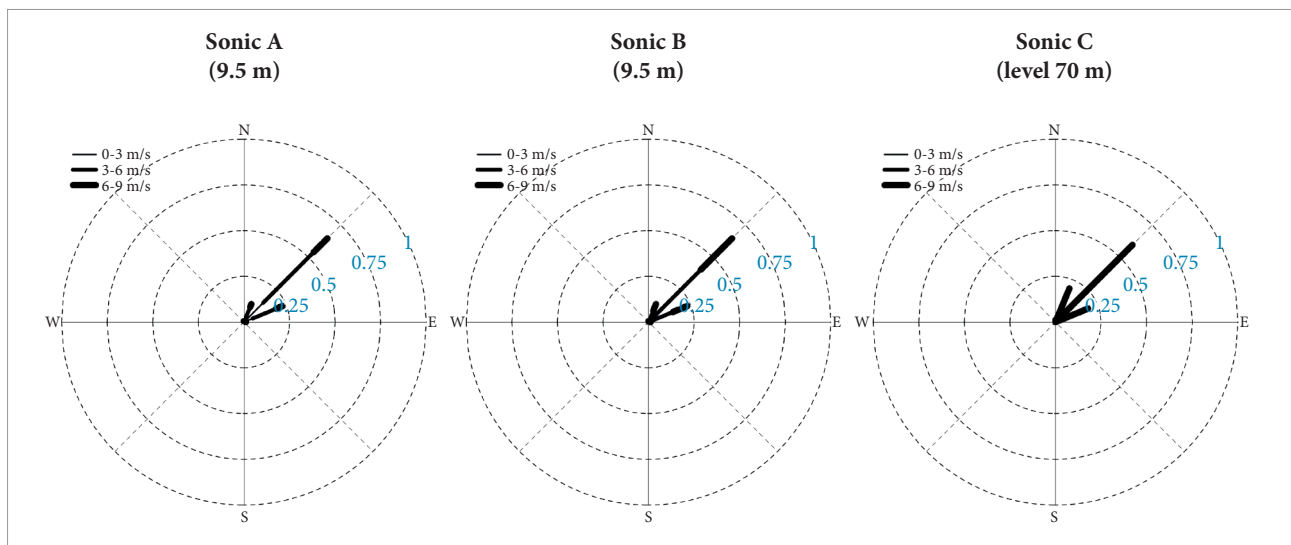


Figure 4. Windroses for Sonic A (700 m inland), Sonic B, and for the anemometer at the top of the tower. Sonic A was 700 m inland, and Sonic B plus tower was 750 m inland.



Figure 5. Sonic A mounted on a mast 9.5 m above ground level at a clearing site with sparse short grass, and lower panel shows Sonic B mounted at the same height but on a tower, with upwind fetch composed by dense bushes of 3 m height.



Figure 6. Aerial photo of the region where the tower, the two Sonics (A and B), and the SoDAR were located. This picture was taken in 2003 just after an accident with a rocket. By 2008, the burnt vegetation (black area near Sonic A and building) had recovered and the damaged buildings were removed from the site. The dashed lines indicate the distance between the tower and Sonic B and Sonic A (227 m), between tower and SoDAR (402 m), and the upwind distance between Sonic A and natural vegetation (20 m).

prevailing wind, there is an upwind fetch of 20 m, which is half composed by sparse short grass and half by asphalt. Beyond that, the fetch is composed by same natural vegetation that is present at Sonic B's site. At the tower there is no surface cover change for a fetch of at least 200 m long. Note that these details are also presented in Fig. 5, and we are excluding most part of the slope of the escarpment in the discussion of the fetch here.

The wind profile at the tower is permanent, but the two Sonics were temporary and operated from September 17–25, 2008. This period of two weeks is within the dry season in the region, and according to Fisch *et al.* (2010) is when the easterly winds are the strongest (10–15 m/s). The wind speed and wind direction data from the profile are sampled at 2 seconds but only 10-minute averages are kept. All turbulent fluxes refer to correlation of velocity with velocity, and velocity with temperature during half-hour periods. The Reynolds mean removal was done using 30-minute block averages, and fluctuations were obtained by subtracting the average values from the instantaneous values. Near the observation points the surface was flat and only horizontal rotation was applied to align the x-axis of the reference frame with the direction of the mean wind. Because there was no fast response humidity and pressure measurements available, we approximated the

buoyancy flux $\overline{w'\theta'_v}$ by the virtual sonic temperature flux $\overline{w'T'_{sv}}$. Where w' , θ'_v and T'_{sv} are, respectively, fluctuations of vertical wind velocity, virtual potential temperature, and derived sonic virtual temperature. We are aware of the error we may introduce when doing such approximation. Fluctuations of virtual temperature T'_v are not exactly the same as T'_{sv} . Nonetheless, fluctuations of sonic virtual temperature are sensitive to fluctuation of humidity as does virtual temperature, but in T'_v the influence of humidity fluctuation is slightly higher. There exists also influence of pressure fluctuation on the buoyancy flux, but we believe it is negligible. In order to simplify our notation in the whole rest of the text, we have dropped the letter “s” in the subscript of $\overline{w'T'_{sv}}$.

Wind data from an acoustic Doppler detecting and ranging device – SoDAR (from Atmospheric Systems Corporation with frequency operation range between 4500 and 5500 Hz) were used as complementary data for this study. The wind profiler (SoDAR) operated from October 11 to 14 of 2011, and was located inside a second clearing (Fig. 6) at 6 m east and 402 m north from the tower, approximately 675 m from the ocean (Fig. 3).

RESULTS

INTERNAL BOUNDARY LAYERS

The windroses (Fig. 4) obtained from the tower top level (70 m) aerovane, and from both sonics indicate that the average flow direction is approximately uniform within the height of the tower and within the horizontal extension of the experimental array size. The wind is predominantly from the sector north-north-east (NNE), with ~ 70% of the time with winds coming from NE. This result is somewhat similar to what Gisler *et al.* (2011) found using a longer wind data set. They showed that for dry season, for a period between the years 1996–1999, the predominant winds were 45% from NE and 40% from ENE, and the remaining 15% from NNE and E. In a scale of about 10 km, the costal line is aligned north-north-west (NNW) – south-south-east (SSE), and winds reaching the tower and Sonic A are necessarily from the ocean (Fig. 2). Because in the direction NE to SW the surface drastically changes, the lower part of the marine boundary layer develops an IBL when it reaches the coast (Arya, 2011). Using the IBL formula $z_{IBL} \approx A z_{OL}^{0.2} x^{0.8}$ (Elliot, 1958), with

$A=0.75$ (Walmsley, 1989; Garratt, 1990) and a roughness length (z_0) of 0.35 m, and the distance from the steepest part of the escarpment to the tower along the predominant wind direction (200 m), gives an IBL of approximately of 42 m deep at the tower. The 0.35 m roughness length z_0 was obtained by adjusting a neutral logarithmic wind profile to the tower (Fig. 7).

Here, we have to point out that the situation is a bit more complicated than the types of IBLs discussed in the literature (e.g., Stull, 1988; Garratt, 1990; Arya, 2001). Besides the surface roughness changes, there is a topographical barrier. According to Marinho *et al.* (2009) the flow obstruction caused by the barrier forces the flow to accelerate and to develop a recirculation. The recirculation train extends from where the plateau levels off to about 200 m inland. However, the average wind vector field for a layer between 30 and 65 m AGL, obtained from the SoDAR data, shows a horizontal flow with no reversal in the flow direction. The main difference between this study and Marinho *et al.* (2009) is that the analysis presented here is based in the real topography with approximately 8 degrees inclination barrier, while in previous it was assumed step-type barrier with 90 degrees inclination. Because in the real situation

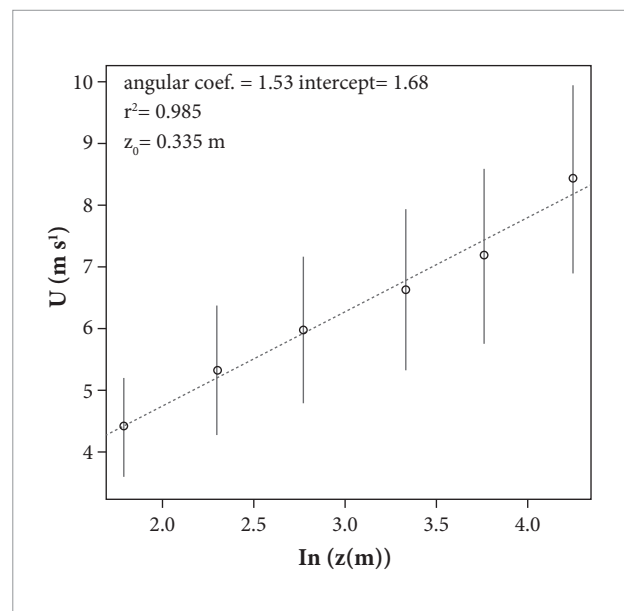


Figure 7. Circles represent tower average wind profile as function of $\ln(z)$. The dotted is a neutral logarithmic curve, $U(z) = (u^*/k) \ln(z/z_0)$, adjusted to the tower profile. The angular coefficient, the linear coefficient, r^2 , and z_0 refer to the dotted line. The upper and lower ends of the vertical solid lines are the speed standard deviation added and subtracted, respectively, from the average speed.

the slope is significantly more gentle and the measuring points were more than 200 m inland from the steepest part of the escarpment, we believe that the recirculation zone, if existent, will be located upwind and the generated wake will be largely diffused by turbulence by the time the flow reaches the observing points. Therefore, the complicating factors added to the flow due to the barrier should not be the cause for different turbulent regimes at the observing points. In addition, because the IBL height (42 m) is above the height of both sonics (9.5 m), the IBL should be close to equilibrium at the sonics, in sense that the flow is not accelerating or decelerating.

Turbulence and Mean Flow State

The first result, one finds when looking to the average time series of wind, friction velocity, $\overline{w'T_v'}$, and turbulent kinetic energy (TKE) for Sonic A and Sonic B (Sonic A is ~ 227 m north of Sonic B), is that the mean wind speed is stronger at Sonic B than at Sonic A (Fig. 8a, b, and c) but u_* and TKE are rather weaker. The friction velocity u_* was obtained through $u_* = \sqrt{-u_r'v_r'}$. The u_r and v_r are, respectively, the velocity components along and perpendicular to mean wind direction, obtained through 2D-horizontal rotation, w the vertical velocity component, and primes denote perturbations. The mean wind

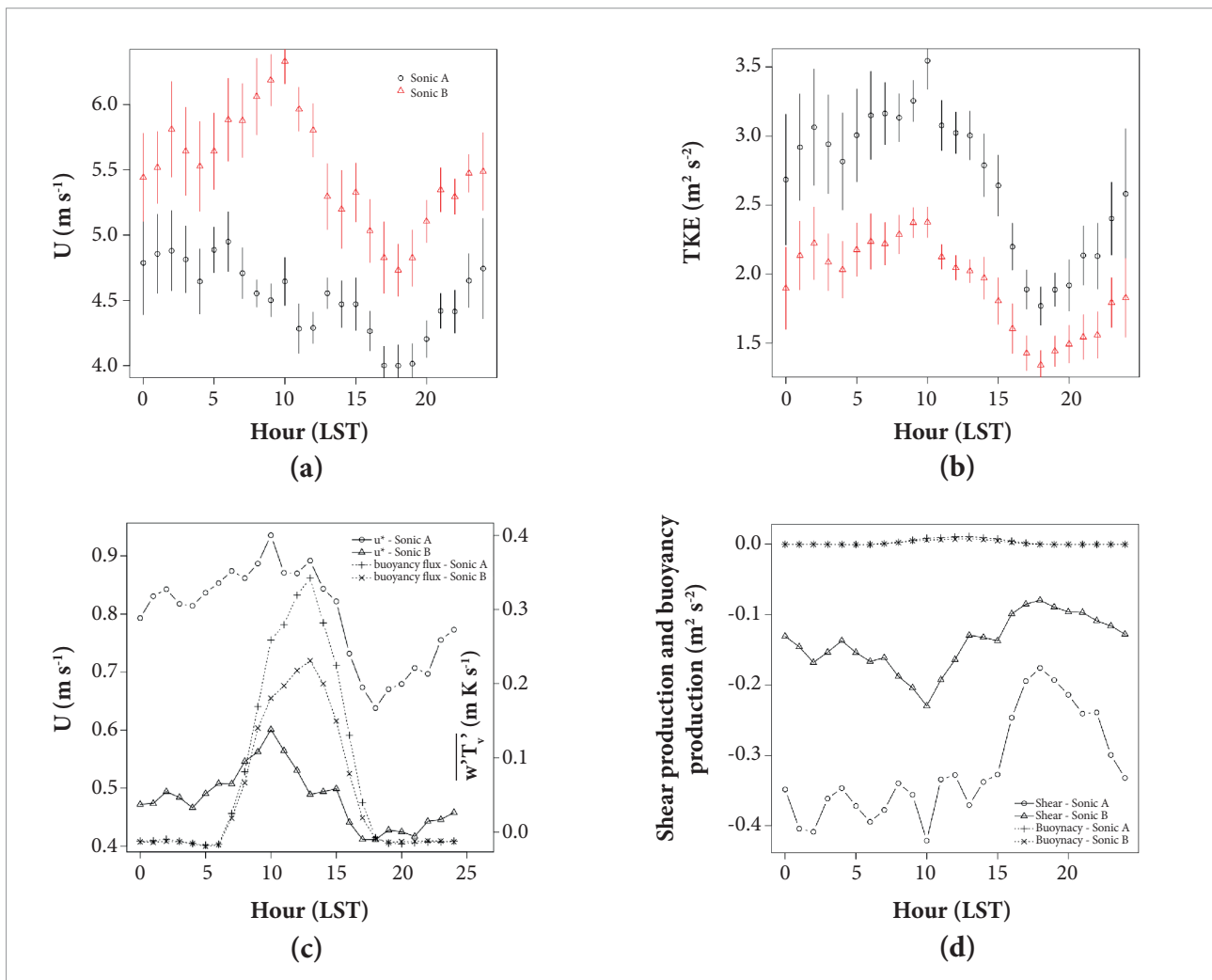


Figure 8. Twenty-four-hour cycles for (a) wind speed for Sonic A (black line) and B (red line), (b) turbulent kinetic energy for Sonics A and B, (c) friction velocity u_* and buoyancy flux $\overline{w'T_v'}$ for sonics A and B, and (d) shear production, and buoyancy production/destruction terms for Sonics A and B. The vertical bars in (a) and (b) are the standard errors. Each point refers to 1-hour bin-averages with 18 data points. The error bars include natural variability of the flow and instrumentation errors as well. However, differences between measurements, caused by instrumentation errors, should be minimal because sensors were kept the same.

was obtained through $U = \overline{u}$, and $TKE = 1/2 (\overline{u'^2} + \overline{v'^2} + \overline{w'^2})$. For all these variables, we used the sonic 10 Hz data. The second result is that, shear production term ($SP = \overline{u_r' w'} \partial U / \partial z$), and buoyancy production/destruction term ($BPD = (g/T_{ref}) \overline{T_v' w'}$) are smaller at Sonic B than at Sonic A (Fig. 8d). The vertical gradient of the horizontal wind was determined using the U , and the sonic measuring height (9.5 m AGL). Velocity at the surface was set equal to zero. Having in mind that origin of the wind (e.g., pressure gradient and advection of momentum) was the same and that the measurements were taken at the same height AGL at Sonic A and B, these results clearly show the consequence of stronger turbulence at Sonic A. It has to be recalled that Sonic A was located in clearing and Sonic B was not. Wind speed, TKE , and BPD at the tower (Sonic B) and clearing (Sonic A) come somewhat closer only at night (1700–0500 local standard time (LST)), when the layer is weakly stable. Sonic B shows wider distribution than Sonic A for the stability parameter (z/L), indicating that the flow regime at the tower is less neutral than at the clearing as is presented in Fig. 9. Here, L is the Obukhov length ($L = u_*^3 / k (g/T_{ref}) \overline{w' T_v'}$, where k is the Von Karman constant = 0.4) and $z=9.5$ m, is the height AGL of the sonics. Values of z/L at Sonic A resemble more the values found within the surface layer closer to the surface, with wind shearing being the dominant source of turbulence and buoyancy a secondary source. At the tower it resembles more

the turbulence found over higher levels in the boundary layer, with somewhat diminished influence of wind shearing on the generation of turbulence.

The wind speed, TKE , SP , and BPD show a clear diurnal cycle, peaking in the morning before noon and being a minimum around 1800 hours of LST. Note though that in SP there is a negative peak, with this variable almost completely mirroring wind and TKE . In the TKE budget equation there is minus sign in front of SP , which makes this terms always production term. The objective here is not to close the TKE equation, but rather to quantify the sources of turbulence generation, SP and BPD at the clearing and tower, which makes the turbulence at these places to be distinct. At the clearing, SP and TKE are in phase with each other but wind is not so. Between 0500 and 1000 LST there is a clear decreasing tendency for the wind but not so for SP . Note that just after 0500 LST the wind is maximum but SP is not. Shear Production (Fig. 8d) only becomes a maximum at 1000 LST, when the wind is weaker. The lack of clear tendency in SP and the apparent tendency for wind to decrease between 0500 and 1000 LST might be a result of averaging a small data record. Nine days of data were necessarily a small sample. In fact, when plotting the entire time, wind series (result not shown), we do see it increasing during this period for a few days. Perhaps, an entire dry season period would be enough to show that U increases between 0500 and 1000 LST. Beyond 1000 LST the wind and SP become stronger and negatively related (Fig. 8a and d), meanwhile TKE seems to be slightly less dependent on SP . Just after 1000 LST TKE decays not following the increase in decay in SP , but further on until 1500 LST it levels off while wind and SP vary. During this period the BPD is strongest and it probably helped to keep TKE near constant. At the tower there is a similar situation. Immediately after 1000 LST, wind and SP decrease forcing TKE to diminish. Beyond this point until 1500 LST, the approximately constant values of TKE are partially kept by the strong BPD . As a bottom line, we can conclude that the main difference between the clearing and the tower is that, there is stronger turbulence at the former. The fact that the U , SP , and TKE are not in phase with each other is consequence of sampling a small data record. The observed 24-hour wind cycle maybe a result of effects of variable local horizontal temperature gradient (sea breeze) interacting with the local trade winds. In a recent study conducted at the costal and central regions of Maranhão State, Medeiros and Fisch (2012) observed that 24-hour wind hodograph was the result

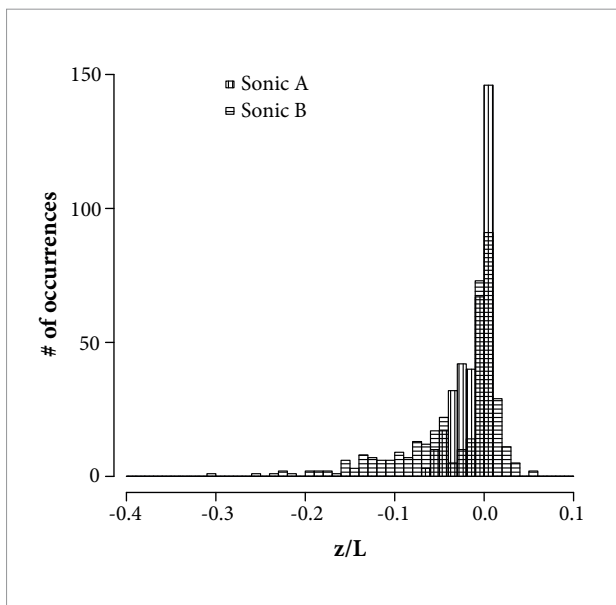


Figure 9. Distribution of z/L stability parameter for Sonics A and B. All cases were included.

of the sea breeze interacting with a large-scale southerly flow during the dry season.

Spectra

The normalized spectra $f S_\alpha / (u_*^2 \phi_\varepsilon^{2/3})$, where $\alpha = u_r, v_r$, and w , reveals that at Sonic B the turbulence spectral peak is at low frequencies while at Sonic A the peak is displaced towards high frequencies. This result is clearly seen in Fig. 10, longitudinal velocity u_r (along mean wind direction) and lateral velocity v_r (crosswind – result not shown) but not in the vertical (w) velocity (Fig. 11). Such differences indicate that at Sonic A site turbulence is more fully developed because of higher SP . Turbulence at Sonic B is less isotropic than at Sonic A, its w -spectrum shows an inertial, but its u -spectrum has neither subinertial range nor constant slope at high frequencies. The normalized TKE dissipation rate, $\phi_\varepsilon = kz\varepsilon/u_*^3$, was determined by adjusting through least-square method $f S_u / u_*^2 = 0.3 \phi_\varepsilon^{2/3} n^{-2/3}$ (Kaimal and Finnigan, 1994) to the inertial subrange of u_r -spectrum, where n is the normalized frequency (fz/U),

and f is the frequency in Hertz. The ϕ_ε was calculated for every 30-minute spectrum and later used to obtain the 30-minute normalized spectra of u_r, v_r , and w , which were finally averaged (Figs. 10 and 11). Turbulence mechanically generated (e.g., through SP) has spectrum concentrated at higher frequencies interval than do turbulence generated by convection (e.g., through BPD). The SP supplies energy directly to u_r and BPD to w , therefore the shifting in u_r -spectrum is a direct consequence of stronger SP . For the remaining spectral components (w and v_r), it is an indirect consequence, because they have their energy supplied by correlation pressure term, which is a term that works in a way to make the turbulence more isotropic by removing energy from u_r and putting in w and v_r .

Combining the average wind speed with the inverse of the u_r spectral peak frequency, one finds that typical scale size of horizontal eddies are in the order of 50 m for A and 120 m for B. Consequently the clearing, which is less than 100 m wide, should not support the typical eddy sizes present at B. Its presence not only caused higher $\overline{u_r'w'}$ $\partial U/\partial z$ and

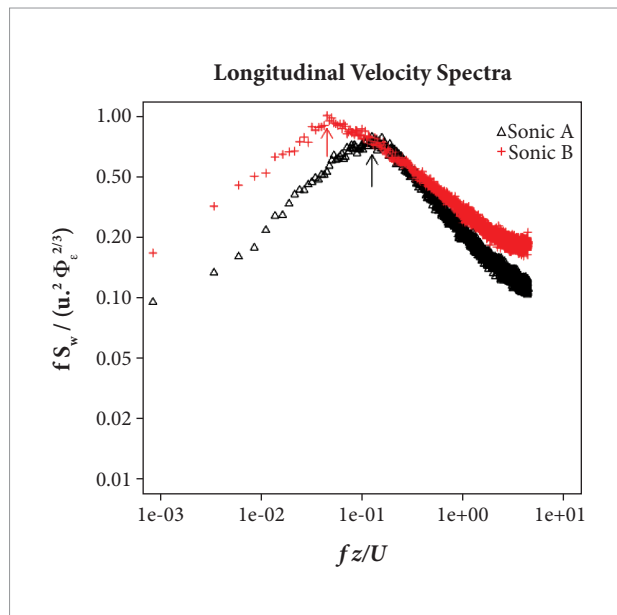


Figure 10. Normalized u -spectral energy density as a function of normalized frequency ($n = fz/U$). Each point represents a binned average of all 30-minute spectra. The bins were defined by constant increments in n . The shifting in the spectral peak of u from Sonic A to Sonic B is 0.044 Hz and in v is 0.061 Hz.

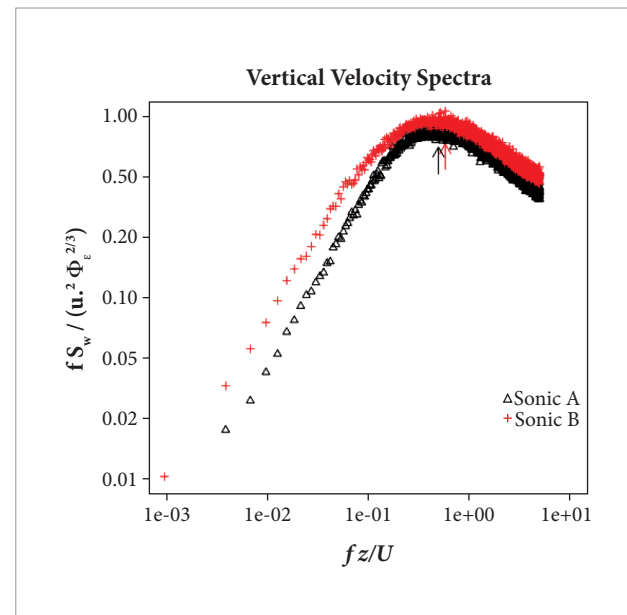


Figure 11. Normalized w -spectral energy density as a function of normalized frequency ($n = fz/U$). Each point represents a binned average of all 30-minute spectra. The bins were defined by constant increments in n . The shifting in the spectral peak of w from Sonic A to Sonic B is 0.021 Hz.

stronger mechanical turbulence, as consequence of a wake behind the trees interacting with the mean wind above, but also a restrictive factor for the size of the horizontal eddies.

WIND SPATIAL REPRESENTATIVENESS

Wind measurements taken 30 and 70 m AGL at the tower and at nearby SoDAR during the dry season 2011 (October 11–14), plus the wind measurements taken by Sonics A and B at 9.5 m AGL during the dry season of 2008 (period of Murici II experiment, September 17–25), were used to define the spatial representativeness of the wind at CLA. The 10-minute wind averages were used for the comparison. The parts of the whole data set came from two different years. However, because surface cover did not change and the wind direction and speed of the prevailing winds, during the measuring period in 2008 and 2011, were very similar, this time period difference should not compromise the analysis. The same level wind measurements were compared through the usage of the statistical indices correlation, normalized mean square error, and fractional shift presented in Table 1 (see caption for details). Although the comparison for the levels 70 and 30 m had the largest distance (402 m) and the measuring techniques were distinct (SoDAR and tower), the 70 m had the best values (scores) for the statistical indices among all. The worst scores obtained for 30 m are partially an experimental artifact caused by different equipments, and the

slightly better scores for the 9.5 m are due to identical equipments, and perhaps shorter distance 227 m (Fig. 6).

The results showed that 70 m wind level is more uniform across the region. Surface inhomogeneities, like the clearing where Sonic A was located and the second clearing, where the SoDAR was located (see Fig. 6 for details), have less influence at this level as one would expect. This height is near the top of the calculated IBL, and it is possible that it is above the first real IBL, which forms near the edge of the plateau. The 30-m results indicate that this level is the least spatial homogenous; however, because of the problems mentioned above we still believe that the 30 m level is spatially more homogenous than the 9.5 m level.

CONCLUSION

Even though the experimental array was limited, two places with turbulence measurements, and the campaign duration was short, less than two weeks, we can still draw some qualitative and quantitative conclusions. For a distance of 200 m (Fig. 3) downwind from the edge of the escarpment, near-surface turbulence is not spatially homogeneous at CLA launching pad site. It is a consequence of the development of other IBL at the clearing, internally to a first one, which develops when

Table 1. For the 70 m and 30 m levels, the tower 70 m and 28 m wind measurement levels were compared with the 30 m and 70 m of the SoDAR. The SoDAR was located 402 m north from the tower (Fig. 6) and operated at that location from October 11 to 14, 2011. For the 9.5m level, we used two sonic anemometers 227 m apart, which operated from September 17 to 25, 2008.

	Spatial representativeness of the wind					
	Zonal wind speed (\bar{U})			Meridional wind speed (\bar{V})		
Measurement height (m)	9.5	30	70	9.5	30	70
Distance between measuring points (m)	227	402	402	227	402	402
Correlation*	0.81	0.75	0.83	0.87	0.76	0.83
Normalized mean square error**	0.04	0.02	0.01	0.03	0.03	0.02
Fractional shift***	0.79	-0.63	-0.32	0.34	0.21	0.08

*The correlation was determined by $\frac{\sum_{i=1}^N [x_i - \bar{x}][y_i - \bar{y}]}{\sigma_x \sigma_y}$, where x_i and y_i represent, respectively, the i -th measurement from two different sensors, and σ_x and σ_y standard deviations of x and y sensors. Optimum value is one.

** Normalized mean square error was computed by $\frac{\sum_{i=1}^N [x_i - y_i]^2}{N \bar{x} \bar{y}}$. Optimum value is zero.

*** Fractional shift was computed by $2(\sigma_x - \sigma_y) / (\sigma_x + \sigma_y)$. Optimum value is zero.

the wind first encounters the escarpment. Due to our limited experimental array, we could not determine the extension of the first and second IBLs. *TKE*, shear, and buoyancy are different even within a distance of 227 m (Fig. 6). The point closer to the escarpment (Sonic A), but in a clearing, had stronger u , *TKE*, *SP* (also true for momentum flux), and buoyancy flux (buoyancy production term) but weaker wind. Part of the increment of *TKE* at the tower and clearing during the sunlight hours, was due to stronger buoyancy flux. The stronger buoyancy at the clearing must have been a consequence of the asphalt's higher surface temperature, upwind inside the clearing. The presence of the clearing was also the reason for higher u and weaker wind. We suppose that a wake zone is developed behind trees, that delimit the clearing perimeter, and it interacting with the mean wind increased the removal of momentum from it.

As a bottom line of this analysis, the wind, *TKE*, and fluxes measured at the tower are not representative of the conditions at the clearing where the rocket launcher is located. Nonetheless, in the absence of better measurements, the spatial analysis of the wind components ($\overline{U}, \overline{V}$) showed that the tower top-level (70 m)

wind might be the least surface affected measurement. It can be used as a first approximation to represent the wind for the region at that level, relative to operational decisions concerning rocket launch and diffusion of pollutants exhausted by the rockets.

ACKNOWLEDGMENTS

The authors acknowledge the financial support from the Conselho Nacional de Desenvolvimento Científico e Tecnológico (CNPq) under the grants 510159/2010-9 (Medeiros), PQ 303720/2010-7 (Fisch), 471143/2011-1 (Marciotto), and Fundação de Amparo a Pesquisa do Estado de São Paulo (2010/16510-0). The authors are also thankful to NASA Land Processes Distributed Active Archive Center (LPDAAC); ASTER L1B; USGS/Earth Resources Observation and Science (EROS) Center, Sioux Falls, South Dakota 2001 for providing the topographic data. The authors also acknowledge the valuable suggestions made by reviewers to make the work better.

REFERENCES

- Arya, S.P., 2001, Introduction to Micrometeorology. Academic Press, San Diego.
- Case, J.L., Wheeler, M.M., Manobianco, J., Weems, J.W. and Roeder, W.P., 2005, A 7-yr climatological study of land breezes over the Florida spaceport. *Journal of Applied Meteorology*, Vol. 44, No. 3, pp. 340-356.
- Elliot, W.P., 1958, The growth of the atmospheric internal boundary layer. *Transactions of the American Geophysical Union*, Vol. 39, No. 6, pp. 1048-1054.
- Fisch, G., Avelar, A.C., Marinho, L.P.B., Gielow, R., Girardi, R.M. and Souza, L.F., 2010, The internal boundary layer at the Alcântara space center: wind measurements, wind tunnel experiments and numeric simulations. In: *Proceedings of the Fifth International Symposium on Computational Wind Engineering (CWE2010)*, Chapel Hill, North Carolina, USA May 23-27, 2010.
- Garratt, J.R., 1990, The internal boundary layer – A review. *Boundary-Layer Meteorology*, Vol. 50, No. 1-4, pp. 171-203.
- Gisler, C.A.F., Fisch, G. and Correa, S. C., 2011, Statistical analysis of wind profile in the surface layer at the Alcântara launching center. *J Aerospace Management*, Vol. 3, No. 2, pp. 193-202. doi: 10.5028/jatm.2011.03022411
- Kaimal J.C. and Finnigan, J.J., 1994, Atmospheric boundary layer flows – their structure and measurement. Oxford University Press, New York.
- Mahrt, L. and Vickers, D., 2005, Boundary-layer adjustment over small-scale changes of surface heat flux. *Boundary-Layer Meteorology*, Vol. 116, No. 2, pp. 313-330.
- Marciotto, E.R., Fisch, G. and Medeiros, L.E., 2012, Characterization of surface level wind in the Centro de Lançamento de Alcântara for use in rocket structure loading and dispersion studies. *J Aerospace Technology and Management*, Vol. 4, No. 1, pp. 69-79. doi: 10.5028/jatm.2012.04014911
- Marinho, L.M.B., Avelar, A.C., Fisch, G., Roballo, S.T., Souza, L.F., Ralf, G. and Girardi, R.M., 2009, Studies using wind tunnel to simulate the atmospheric boundary layer at the Alcântara Space Center. *J Aerospace Technology and Management*, Vol. 1, No. 1, pp. 91-98. doi: 10.5028/jatm.200901019198
- Medeiros, L.E. and Fisch, G., 2012, Low atmospheric flow at Centro de Lançamento de Alcântara (CLA) and surrounding areas of the north part of the Maranhão State. In: *Proceedings of the XVII Congresso Brasileiro de Meteorologia*, Gramado, RS, Brazil.
- Merceret, F.J., 2006, Rapid temporal changes of boundary layer winds. *Journal of Applied Meteorology and Climatology*, Vol. 45, No. 7, pp. 1016-1020.
- Moreira, D.M., Trindade, L.B., Fisch, G., Moraes, M.R., Dorado, R.M. and Guedes, R.L., 2011, A multilayer model to simulate rocket exhaust clouds. *J of Aerospace Technology and Management*, Vol. 3, No. 1, pp. 41-52. doi: 10.5028/jatm.2011.03010311
- Stull, R.B., 1988, An introduction to boundary layer meteorology. Kluwer Academic Publishers, Dordrecht.
- Walmsley, J.L., 1989, Internal boundary layer height formulae – a comparison with atmospheric data. *Boundary-Layer Meteorology*, Vol. 47, No. 1-4, pp. 251-262.